TRENDS IN SCIENCES 2025; 22(12): 10751
https://doi.org/10.48048/tis.2025.10751 RESEARCH ARTICLE

Mechanistic Insights into Adsorption of Methylene Blue and Methyl Orange Using Cassava Rhizome Activated Carbon: Adsorption, Characterization and Reusability

Suchada Sawasdee* and Prachart Watcharabundit

Department of Chemistry, Faculty of Science and Technology, Thepsatri Rajabhat University, Lopburi 15000, Thailand

(*Corresponding author's e-mail: suchada.s@lawasri.tru.ac.th)

Received: 23 May 2025, Revised: 23 June 2025, Accepted: 30 June 2025, Published: 10 September 2025

Abstract

This study produced activated carbon from residual cassava rhizome using H_3PO_4 activation at 500 °C. The adsorbent was characterized via nitrogen adsorption-desorption, Fourier transform infrared spectroscopy, X-ray fluorescence spectroscopy, X-ray diffraction spectroscopy and scanning electron microscopy. Adsorption of methylene blue and methyl orange was examined using the batch method, with influencing factors including pH, contact time, initial dye concentration, and temperature. Optimal adsorption occurred at pH 9 and 360 min for methylene blue and pH 2 and 240 min for methyl orange. The Langmuir isotherm best described the adsorption behavior, yielding maximum capacities of 29.154 and 28.736 mg/g at 30 °C, respectively. Kinetic analysis confirmed the pseudo-second-order model for both dyes, while thermodynamic evaluation indicated an endothermic and spontaneous process at higher temperatures. Adsorption mechanisms involved Yoshida hydrogen bonding, dipole-dipole hydrogen bonding, n-π and π-π interactions, electrostatic interactions, ion exchange and pore filling. The adsorbent demonstrated efficient reusability through five cycles, employing 0.1 M HCl for methylene blue and 0.1 M NaOH for methyl orange removal. These findings suggest cassava rhizome-derived activated carbon as a cost-effective alternative for dye removal from aqueous solutions.

Keywords: Cassava rhizome-activated carbon, Methylene blue and methyl orange dyes, Adsorption, Mechanism, Reusability

Introduction

A significant challenge for many nations is achieving coordinated, comprehensive and sustainable water management. A wastewater treatment measure is essential to sustainable water management and is crucial for properly controlling wastewater and water quality [1]. The increasing rate of water contamination brings significant attention to wastewater treatment. Industrial wastewaters typically contain toxic and hazardous substances that are particularly harmful to living organisms; thus, effluents from the food, pharmaceutical, textile, plastic and metal sectors are major contributors to water pollution [2]. Approximately 70 million tons of dyestuff are generated annually due to the widespread application of synthetic dyes and pigments across various global industries [3]. The color of the water is the principal indicator of its quality. Even at minimal dye concentrations (below 1 ppm), the water appears undesirable [4].

Methylene blue (MB) is a widely used cationic dye employed in chemical indicators, coloring agents, and biological dyes. The concentration of MB in different industrial effluents fluctuates based on the specific processes employed. Wastewater generated from textile dyeing and printing may include substantial concentrations of MB, varying from 10 to 1000 mg/L. Releasing wastewater containing MB into natural water bodies may harm ecosystems and aquatic life. The implications of MB-saturated wastewater on human health are very alarming. It is widely acknowledged that MB is detrimental to aquatic organisms, including fish, algae and invertebrates. [5]. Methyl orange (MO) is a prevalent anionic dye primarily utilized as an indicator

in scientific assays and as a coloring agent in the textile industry. Wastewater containing MO is not highly conducive to chemical or biological treatment. MO possesses the potential to be genotoxic and carcinogenic, harming both aquatic organisms and human health [6].

Among existing treatment technologies, adsorption stands out due to its simplicity, cost-effectiveness and environmental compatibility. Adsorption, a surface phenomenon where the adsorbent's surface is coated with the adsorbate, is particularly noteworthy. The adsorption efficiency is significantly influenced by the adsorbent's development and the choice of precursor material. However, the most effective adsorbents are readily available, cost-effective, easy to produce, insoluble, environmentally friendly, non-toxic and efficient [7]. Activated carbon is a widely studied and utilized adsorbent, owing to its high surface area, varied functional groups and favorable physicochemical properties [8]. While commercial forms remain highly effective, their elevated cost hinders large-scale use in wastewater treatment. To enhance performance, activated carbon is often chemically modified to improve surface structure and functionality [7]. The activation process typically involves reagents such as phosphoric acid, zinc chloride, or potassium hydroxide, which promote pore development and increase adsorption capacity. Among these, phosphoric acid is considered more environmentally benign than zinc chloride and operates at lower activation temperatures compared to potassium hydroxide [9].

Researchers have recently endeavored to develop economical adsorbents from agricultural byproducts to eliminate various pollutants from wastewater and water [10]. Using agricultural waste as a precursor for activated carbon production presents the benefits of being ecologically sustainable, renewable and biodegradable [11,12]. Kanyakam *et al*. [13] synthesized activated carbon from cassava rhizome via carbonization at 300 - 600 °C, identifying 400 °C as optimal, yielding a 95.32% methylene blue removal efficiency. Phuriragpitikhon *et al*. [14] employed $ZnCl_2$ and $ZnCl_2/FeCl_3$ as activating agents for cassava rhizome, producing activated carbons with surface areas of 1405 and 554 m^2/g, respectively. Tan *et al*. [15] prepared activated carbon from passion fruit leaves using NaOH for the adsorption of AB113 and methylene blue, attributing the mechanism to electrostatic attraction, hydrogen bonding and π–π interactions. Similarly, Tran *et al*. [16] utilized steam activation and proposed multiple mechanisms for cationic dye adsorption, including dipole–dipole and Yoshida hydrogen bonding, *n*–π interactions, π–π stacking and pore filling.

In Thailand, cassava rhizome (CR) is a prevalent agricultural waste biomass. The CR is the underground part of the stem that produces roots and shoots. The population is largely engaged in agriculture and a significant amount of cassava is cultivated. In 2020, Thailand generated 29 million tons of cassava products, with an expected 6 million tons of CR [17]. Open combustion has typically been employed to dispose of CR, leading to significant environmental problems, particularly an increase in airborne PM10/PM2.5 fine particulate matter [18]. Cassava residues are abundant in lignocellulosic material and are utilized as adsorbents for removing organic and inorganic pollutants in water [19].

Despite extensive studies on cassava-based activated carbon, research remains limited regarding the simultaneous adsorption of both MB and MO, particularly in competitive binary systems. This study addresses that gap by developing activated carbon from cassava rhizome waste and evaluating its performance in removing MB and MO under varying operational conditions – pH, contact time, concentration and temperature. Furthermore, the adsorption mechanisms are elucidated via surface characterization techniques (BET, FTIR, XRF, XRD, SEM) and the material's reusability is assessed through multiple cycles. The findings aim to support the development of efficient, low-cost and sustainable adsorbents for dye-contaminated water, aligning with global water sustainability goals.

Materials and methods

Preparation of activated carbon

Cassava rhizomes (CV) were obtained from Chai Badan District, Lopburi, Thailand. The CVs were cleaned with tap water and subsequently dried in the sunlight. To initiate the activation process, the CVs were cut into small fragments and immersed in 1.0 M phosphoric acid at a ratio of 1:20 (g:mL) for 24 h. The

samples were dried in a hot-air oven at 100 °C for 48 h. The dehydrated cassava rhizome char was then burned at 500 °C for one h in a furnace. Subsequently, it was rinsed with distilled water until the pH attained 7. The activated carbon-cassava rhizome (AC-CR) was desiccated at 100 °C, pulverized in a blender and sifted to achieve a particle size of 150 - 300 µm. Ultimately, it was preserved in a desiccator for subsequent utilization.

Preparation of adsorbate

The adsorbates used were methylene blue (MB) dye (Molecular Formula $C_{16}H_{18}N_3SCl$, molecular weight = 319.98 g/mol) and methyl orange (MO) dye (Molecular Formula $C_{14}H_{14}N_3SO_3Na$, molecular weight = 327.34 g/mol). They were sourced from Merck in Germany. Each amount of dye was dissolved in double-distilled water to achieve a concentration of 100 mg/L, which was then diluted to the required concentrations. All reagents used, including Na_2CO_3, $NaHCO_3$, NaOH and HCl, were of analytical grade and used without further purification. **Figure 1** shows the molecular structure of MB and MO.

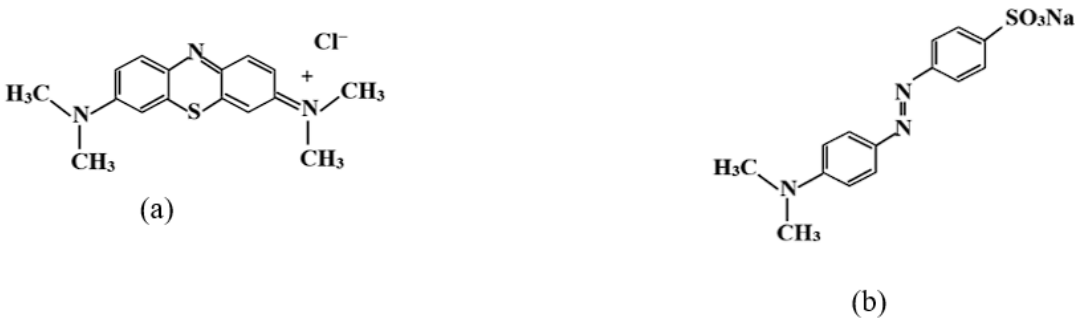

Figure 1 MB (a) and MO (b) structures.

Characterization of adsorbent

The adsorbent was characterized using several techniques. A Quantachrome Instruments Autosorb 1 MP gas sorption analyzer (USA) was used for N_2 adsorption-desorption isotherms to determine BJH pore size and BET surface area. Elemental analysis was conducted via XRF (HORIBA MESA-500W, Japan), structural analysis via XRD (Rigaku Smartlab2, Japan), surface morphology via SEM (LEO 1450 VP, Leo, UK), and surface functional group identification via FTIR (Perkin Elmer Model Two, USA).

Determination of pH_{pzc}

The pH drift method was employed to determine the pH at the point of zero charge (pH_{pzc}). A series of 0.1 M KNO_3 solutions with pH values ranging from 2 to 11 was prepared. The pH ($pH_{initial}$) of each KNO_3 solution was measured using a pH meter (Ohaus, USA) after adding 0.1 M HCl and 0.1 M NaOH. Subsequently, 0.1 g of adsorbent was added to each 100 mL of 0.1 M KNO_3 solution and the mixtures were agitated at 150 rpm for 48 h. After filtering the mixtures, the pH (pH_{final}) of the solution was measured. The pH_{pzc} was determined by plotting the curve of each ΔpH (pH_{final} - $pH_{initial}$) against $pH_{initial}$. The pH_{pzc} is the point where the curve of pH_{final} intersects with the horizontal line that $\Delta pH = 0$.

Boehm titration

The Boehm titration is a method for quantifying certain oxygen-containing functional groups—carboxyl, lactones, and phenols—on carbonaceous substances. The groups exhibited differing acid strengths in the following sequence; hydroxyl > lactones and lactol > carboxyl. A precise quantity of AC-CR (0.5 g) was introduced into multiple Erlenmeyer flasks, each holding 50 mL of 0.05 M solutions of Na_2CO_3, $NaHCO_3$, NaOH and HCl. The flasks were positioned in the thermostatic shaker at room temperature for 48 h. The solution was filtered and 10 mL was titrated with 0.05 M HCl and NaOH. We quantified the concentration of acidic surface groups, presuming that NaOH neutralizes carboxylic, phenolic, and lactone moieties. Sodium carbonate (Na_2CO_3) neutralizes lactones and carboxylic acids, whereas sodium bicarbonate ($NaHCO_3$) neutralizes only carboxylic acids. The amount of HCl

enables us to determine the number of fundamental groups [20].

Method

Adsorption study

For every adsorption test, 0.6 g of the adsorbent was introduced into a 250-mL Erlenmeyer flask filled with 100 mL of a dye solution comprising MB and MO. The solution pH was adjusted using 0.1 M HCl and 0.1 M NaOH. The suspended solutions were agitated at 200 rpm in an isothermal shaker (Daihan Scientific, Korea, IS-10R) maintained at a constant temperature for different durations. After a specified duration, the samples were subjected to filtration and the solution's residual dye concentration was quantified using a UV-visible spectrophotometer (Analytik Jena, Specord 210 plus, Germany) at 665 and 465 nm for MB and MO, respectively. All adsorption experiments were conducted in triplicate. The adsorption capacity and percentage were subsequently computed using Eqs. (1) - (2).

$$q_t = \frac{(C_o - C_t)V}{W} \quad (1)$$

$$\% \text{ adsorption} = \frac{(C_o - C_t)}{C_o} \times 100 \quad (2)$$

where C_o (mg/L) is the initial dye concentration, C_t (mg/L) is the concentration at any time, q_t (mg/g) is the amount adsorbed at any time, V(L) is the volume of the solution and W(g) is the mass of adsorbent.

Adsorption isotherm

The adsorption isotherm clarifies the distribution of molecules between the liquid and solid phases at equilibrium during the adsorption process. This study analyzed the adsorption data using the Langmuir and the Freundlich isotherms.

The Langmuir isotherm is expressed in nonlinear and linear forms in Eqs. (3) - (4), respectively.

$$q_e = \frac{q_{max} K_L C_e}{(1 + C_e K_L)} \quad (3)$$

$$\frac{C_e}{q_e} = \frac{1}{q_{max}} C_e + \frac{1}{K_L q_{max}} \quad (4)$$

where C_e (mg/L) is the equilibrium concentration, q_e (mg/g) is the amount adsorbed at equilibrium, K_L (L/g) is the Langmuir constant and q_{max} (m/g) is the maximum adsorption capacity. The essential characteristics of the Langmuir isotherm can be expressed in terms of a dimensionless separation factor (R_L) which is defined by:

$$R_L = \frac{1}{(1 + K_L C_o)} \quad (5)$$

The Freundlich isotherm is expressed in nonlinear and linear forms in Eqs. (6) - (7), respectively.

$$q_e = K_F C_e^{1/n} \quad (6)$$

$$\log q_e = \log K_F + (1/n) \log C_e \quad (7)$$

where K_F (L/g) is the adsorption capacity, and 1/n is the adsorption intensity.

Adsorption kinetics and thermodynamics

The kinetic models

The study of adsorption kinetics can yield significant insights into the adsorption mechanism. The experiment investigates the adsorption capacity of an adsorbate onto an adsorbent across various time intervals. This study employs the pseudo-first-order, pseudo-second-order and intraparticle diffusion models to analyze the adsorption data. Eqs. (8) - (10) describe the linear representations of the pseudo-first-order, pseudo-second-order and intraparticle diffusion models, respectively.

$$\log (q_e - q_t) = \log q_e - \frac{k_1}{2.303} t \quad (8)$$

$$\frac{t}{q_t} = \frac{1}{k_2 q_e^2} + \frac{1}{q_e} t \quad (9)$$

$$q_t = K_{id} (t)^{1/2} + C \quad (10)$$

where k_1 (1/min) and k_2 (g/mg.min) are the rate constants of pseudo-first-order and pseudo-second-order models, respectively. The q_t (mg/g) and q_e (mg/g) are the amounts adsorbed at any time (min) and equilibrium time, respectively. K_{id} (mg/g.min$^{1/2}$) is the intraparticle diffusion rate constant and C is the intercept.

Kinetic validation

To determine which model best describes the adsorption process, one uses Eq. (11) to calculate the normalized standard deviation, or Δqe (%) [21].

$$\Delta q_e\ (\%) = 100 \times \sqrt{\frac{[(q_{t,exp} - q_{t,cal})/q_{t,exp}]^2}{N-1}} \quad (11)$$

where N is the number of data points, $q_{t,exp}$ (mg/g) is the experimental adsorption capacity and $q_{t,cal}$ (mg/g) is the calculated adsorption capacity for the pseudo-first and pseudo-second models.

Thermodynamic parameter of adsorption

The thermodynamic behavior is analyzed to comprehend the variations in Gibbs energy (ΔG), enthalpy (ΔH) and entropy (ΔS) by examining the adsorption of the adsorbate onto the adsorbent's surface. The Gibbs free energy change (ΔG) in the adsorption process can be expressed by Eq. (12).

$$\Delta G = -RT \ln K_c \quad (12)$$

where K_c ($K_c = q_e / C_e$) is the equilibrium constant, R is the gas constant, and T is the absolute temperature. Also, enthalpy (ΔH) and entropy (ΔS) changes can be estimated by Eq. (13).

$$\ln K_c = \frac{\Delta S}{R} - \frac{\Delta H}{RT} \quad (13)$$

ΔH and ΔS can be determined by the linear plot's slope and intercept between $\ln K_c$ and 1/T.

Reusability test

To maximize the efficiency of the prepared activated carbon, it was proposed that the used activated carbon be regenerated for reuse in the adsorption process. The AC-CR used for MB adsorption was desorbed using 0.1 M HCl, while the other used for MO adsorption was desorbed using 0.1 M NaOH. After cleansing the AC with distilled water until its pH stabilized between 6 and 7, we dehydrated it in an oven and preserved it for the next adsorption cycle. The number of adsorption cycles and the percentage of adsorption were recorded.

Binary adsorption test

Binary adsorption plays a vital role in understanding the competitive behavior of multiple pollutants in complex aqueous systems, such as real wastewater. To assess the efficiency of the binary adsorption system for dye removal, methylene blue (MB) and methyl orange (MO) solutions were mixed to 100 mL at concentration ratios of 20:20, 30:20, and 20:30 mg/L, followed by the addition of 0.6 g of AC-CR. In a binary system, the absorbance of components A (MB) and B (MO) was measured at wavelengths λ_1 (665 nm) and λ_2 (465 nm). Dye concentrations were determined utilizing Eqs. (14) - (15) [22].

$$C_{MB} = (k_{MO2}A_1 - k_{MO1}A_2)/(k_{MO1}k_{MB2} - k_{MO2}k_{MB1}) \quad (14)$$

$$C_{MO} = (k_{MB1}A_2 - k_{MB2}A1)/(k_{MO1}k_{MB2} - k_{MO2}k_{MB1}) \quad (15)$$

where k_{MB1} and k_{MO1} represent the calibration constants for dyes MB and MO at $\lambda_{1,max}$ while k_{MB2} and k_{MO2} represent the calibration constants for dyes MB and MO at $\lambda_{2,max}$ respectively.

Results and discussion

Characterization of adsorbent

Surface area, Pore volume and Pore size distribution analysis

The AC-CR was tested for nitrogen adsorption at −196 °C. The data were analyzed for nitrogen adsorption-desorption isotherm and BJH pore size distribution. These results are shown in **Figure 2** and **Table 1**.

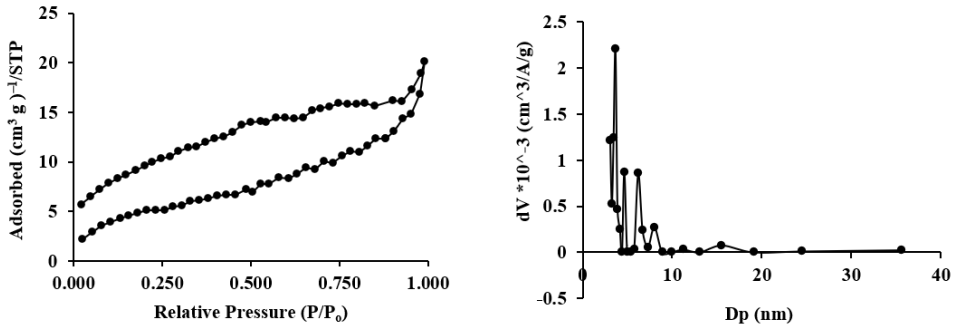

(a) (b)

Figure 2 The plots of nitrogen adsorption-desorption (a) and pore size distribution (b) of AC-CR.

The N_2 adsorption-desorption isotherm of AC-CR, seen in **Figure 2**, exhibits a type IV isotherm with an H4 hysteresis loop. **Figure 2(a)** illustrates that the hysteresis loop features a desorption line plateau between 0.75 to 0.92 P/P_0. This resembles the hysteresis loop observed in activated carbon derived from durian shell waste [23]. Porous adsorbents often display a type IV isotherm during capillary condensation. Consequently, AC-CR ought to serve as the mesoporous adsorbent [24]. The adsorbent exhibiting a type IV isotherm and an H4 loop comprises micropores and mesopores [25,26].

Table 1 Textural parameters of AC-CR.

Parameters	Values
BET surface area (S_{BET}) (m^2/g)	19.738
BET total pore volume (V_p) (cm^3/g)	0.031
BET average pore diameter (D_p) (nm)	6.282
BJH surface area (m^2/g)	11.316
BJH pore volume (cm^3/g)	0.020
BJH median pore diameter (nm)	3.696
BJH pore radius (nm)	1.848

The BET plot (not shown) is used to ascertain the surface area from the nitrogen adsorption-desorption isotherm data. Linear adsorption occurs within the P/P0 range of 0.05 to 0.2, exhibiting a remarkable correlation (R^2) of 0.9998, whereas the BET surface area of AC-CR is 19.738 m^2/g. The BET total pore volume (Vp) of AC-CR is 0.031 cm^3/g. Using the Wheeler Eq. ($Dp = 4,000\ Vp/S_{BET}$) [27], we calculated the BET pore diameter (Dp) to be 6.282 nm. **Figure 2(b)** depicts the BJH pore size distribution, predominantly spanning from 1 to 35 nm, with the median pore size of AC-CR calculated at 3.696 nm. Additional details regarding the BJH surface area, pore volume and pore radius are provided in **Table 1**. The relatively small surface area and moderate pore size of AC-CR indicate that adsorption is likely influenced more by surface chemistry and pore accessibility than by total surface area alone. Despite its limited S_{BET}, the abundance of mesopores (as indicated by BJH analysis) may facilitate the rapid entry and absorption of bigger organic molecules such as methylene blue (MB) and methyl orange (MO). Furthermore, employing phosphoric acid to activate the material introduces functional groups to the surface—specifically phenol and carboxyl groups—that enhance

its interaction with adsorbed molecules, promoting attraction or bonding [28].

Surface oxides in AC-CR can be characterized by Boehm titration. The surface comprises acidic groups (0.83 meq/g)—carboxylic (0.47 meq/g), phenolic (0.32 meq/g) and lactonic (0.06 meq/g)—as well as a negligible amount of basic groups (0.12 meq/g). Acidic groups, including carboxylic, phenolic and lactonic, enhance surface polarity, hence facilitating stronger electrostatic interactions and hydrogen bonding with polar adsorbates such as methylene blue (MB) and methyl orange (MO).

SEM analysis

Figure 3 presents a scanning electron micrograph of the AC-CR adsorbent before adsorption, captured at magnifications of 200 and 1,000x, illustrating that the AC-CR surface had a porous structure with pores exceeding 2 μm in diameter. The AC-CR displays a heterogeneous surface marked by pronounced ridged cavities and its pore size exceeds the molecular diameters of MB (0.81 - 0.91 nm) and MO (1.34 - 1.44 nm) [29].

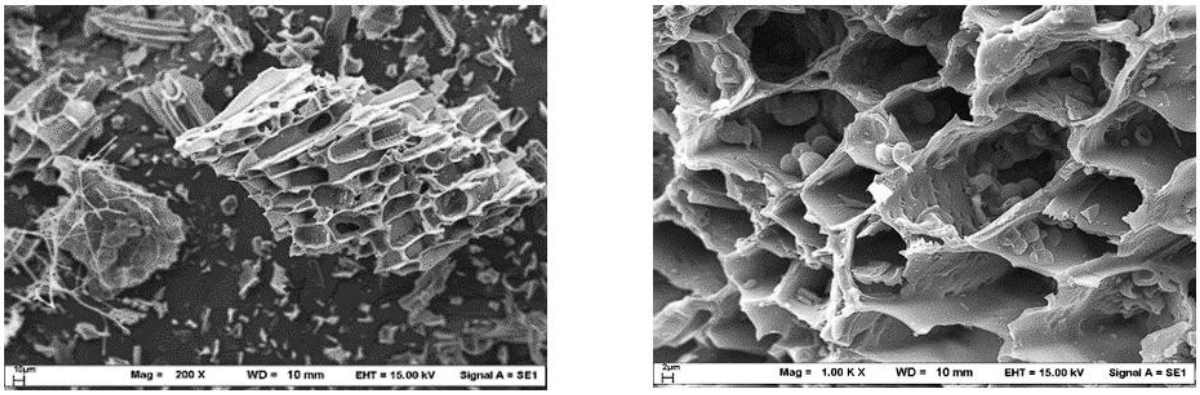

(a) (b)

Figure 3 Scanning electron micrograph of AC-CR adsorbent at 200 (a) and 1000 (b) magnification.

XRF analysis

The XRF spectrophotometer identified the chemical composition on the surface of AC-CR before and after MB and MO dye adsorption. The data revealed that AC-CR had the following elements before adsorption: Ca (57.18%), P (39.36%), Fe (2.10%), Mo (0.57%), Rh (0.49%), Cu (0.19%), Ni (0.17%) and Sr (0.03%). After MB adsorption, the chemical components were as follows: Ca (55.83%), P (40.89%), Fe (1.64%), Mo (0.73%), Rh (0.46%), Ni (0.21%), Cu (0.19%) and Sr (0.05%). The adsorption process reduced the concentrations of Ca and Fe for MB. This is likely due to the adsorption process facilitating the exchange of the dye cation with the cation on the AC-CR surface [30]. The subsequent cation exchange step is crucial to MB's adherence to AC-CR. After MO adsorption, the chemical components were as follows: Ca (38.10%), Cl (39.36%), P (18.15%), Fe (2.37%), Mo (0.81%), Rh (0.79%), Cu (0.39%), Sr (0.03%).

XRD analysis

Figure 4 depicts the XRD examination of the AC-CR before adsorption within the 2θ range of 10° to 80°. Before adsorption, the principal diffraction peaks were observed at 22.87, 24.04, 25.15, 26.60, 29.29, 30.60, 31.60, 50.56, 58.95, and 74.89, with an average crystallite size of 39.85 nm. The carbon predominantly displays an amorphous structure, as evidenced by a large reflection in the 2θ range of 20° to 25°, indicating the amorphous phase [31]. Wang *et al*. [32]. elucidate that the lignin content of the sample signifies the non-crystalline cellulose present in biomass waste.

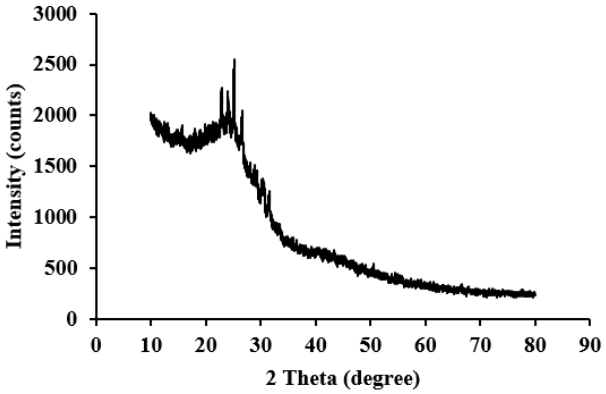

Figure 4 XRD analysis of AC-CR adsorbent.

FTIR analysis

Fourier transform infrared spectroscopy (FTIR) analysis was conducted to ascertain the chemical structure and functional groups present before and after adsorption of MB and MO onto activated carbon (AC-CR), as depicted in **Figure 5**, which illustrates the FTIR spectral range of 4,000 to 500 cm^{-1}.

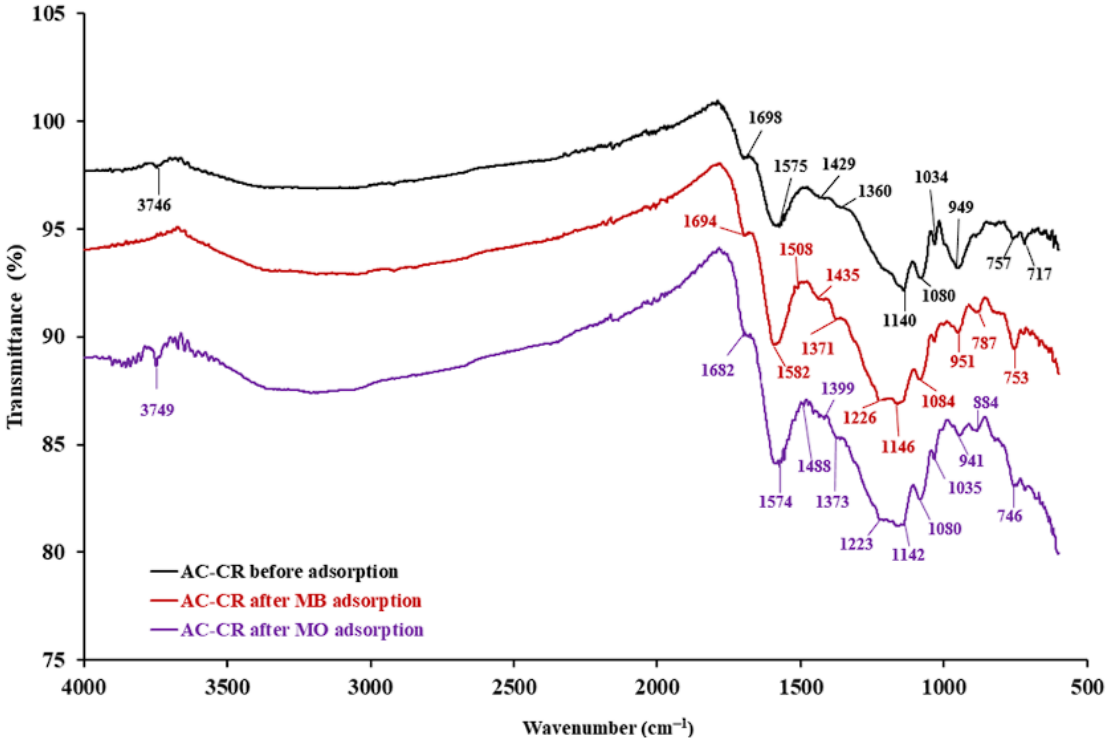

Figure 5 FTIR spectrum of AC-CR before and after MB and MO adsorption.

Before adsorption, the signal at 3,746 cm^{-1} signified the presence of hydroxyl (-OH) groups in phenols, carboxylic acids and water adsorbed on AC-CR [33]. The peaks at 1,698 and 1,575 cm^{-1} corresponded to C=O and C=C vibrations, respectively [34]. The signal at 1,140 cm^{-1} indicated the presence of C–O bonds in polysaccharides such as cellulose and starch, as well as in phenolic, ether and ester functionalities on the surface of AC-CR [8]. Hmamouchi *et al*. [35] identified the broadband range of 1,000 - 1,300 cm^{-1} as indicative of C–O stretching in acids, alcohols, phenols, ethers and esters. The peaks at 1,080, 1,034, 1,140, and 1,220 cm^{-1} confirmed the presence of C–O bonds. The peak at 757 cm^{-1} was attributed to the bending vibration of –C≡C–

H–C–H [36] and the groups substituted aromatic rings [37].

After MB adsorption, the peaks shifted to 2,903, 1,694, 1,582, 1,435, 1,371, 1,226, 1,146, 1,084, 1,035 and 951 cm^{-1}. The peaks for MO adsorption shifted to 3,749, 2,903, 1,682, 1,574, 1,373, 1,142, 1,080, 1,035 and 941 cm^{-1}. Compared to pre-adsorption, additional peaks appeared at 1,508 and 1,226 cm^{-1} for MB adsorption and at 1,488, 1,399 and 1,223 cm^{-1} for MO adsorption. The alteration in absorption peaks indicated that dye molecules interacted with the functional groups of AC-CR [38]. The presence of these functional groups enhanced heterogeneity and consequently, adsorption. The intensity of the signal corresponding to the hydroxyl vibration peak at 3,746 cm^{-1} in the adsorbent decreased or shifted after MB and MO adsorption, indicating the formation of hydrogen bonds between the adsorbent and both dyes [39].

Adsorption study

Effect of pH

The surface charges of the adsorbent in the solution were determined using the point of zero charge (pHpzc). The pHpzc of AC-CR was 5.4, as illustrated in **Figure 6(a)**. The impact of pH, ranging from 2 to 11, was investigated at an initial dye concentration of 50 mg/L, with a contact duration of 360 min at 30 °C. The adsorption data are presented in **Figures 6(b) - 6(c)** for MB and MO, respectively.

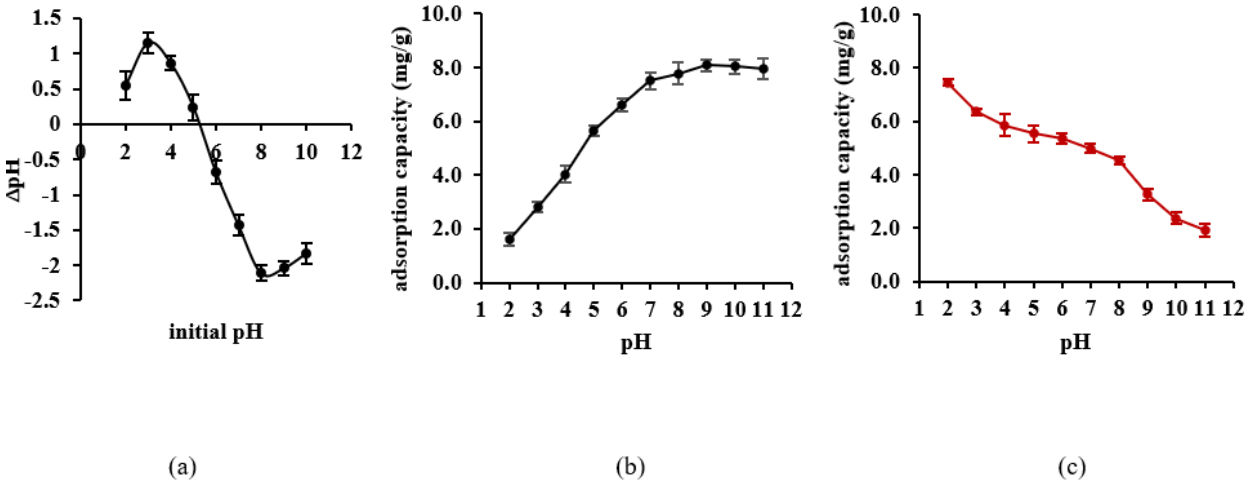

Figure 6 pH_{pzc} determination (a) and effect of pH on MB (b) and MO (c) adsorption.

Figure 6(b) illustrates that as the pH increased from 2.0 to 9.0, the adsorption of MB dye improved. However, the adsorption remained constant when the pH exceeded 9. At pH levels below the pHpzc, the adsorption capacity of the adsorbent diminished due to the repulsion between the positive charge on its surface and the MB cations. When the pH level exceeded the pHpzc, the surface of the adsorbent acquired a negative charge. The negatively charged surface adhered to the positively charged dye (MB^+) molecules due to electrostatic attraction.

The efficacy of AC-CR in eliminating MO dye was maximized at pH 2 and diminished at elevated pH levels, as seen in **Figure 6(c)**. The anionic nature of MO and the protonation state of the functional groups in AC were likely responsible for this pH-dependent adsorption. The maximum elimination occurred at pH 2 due to the attraction between the positively charged AC-CR surface and the negatively charged MO dye.

Effect of contact time and initial dye concentration

Adsorption experiments were conducted with initial dye concentrations of 25, 50 and 100 mg/L at 30 °C, with agitation times ranging from 1 to 540 min. **Figure 7** shows that the adsorption capacity increased with contact time and dye concentration, occurring rapidly within the first 15 min. Over 360 min, the MB adsorption capacity rose to 4.231, 7.997 and 12.504 mg/g. At the equilibrium time of 240 min, the MO

adsorption capacity reached 3.815, 7.542 and 11.993 mg/g for respective dye concentrations. The initial rapid adsorption is attributed to abundant surface sites, while the later slower rate is likely due to repulsive forces between adsorbed and free dye molecules [5]. At equilibrium, the interactions of the adsorbent and mass transfer are strengthened due to increased diffusion at elevated dye concentrations [40].

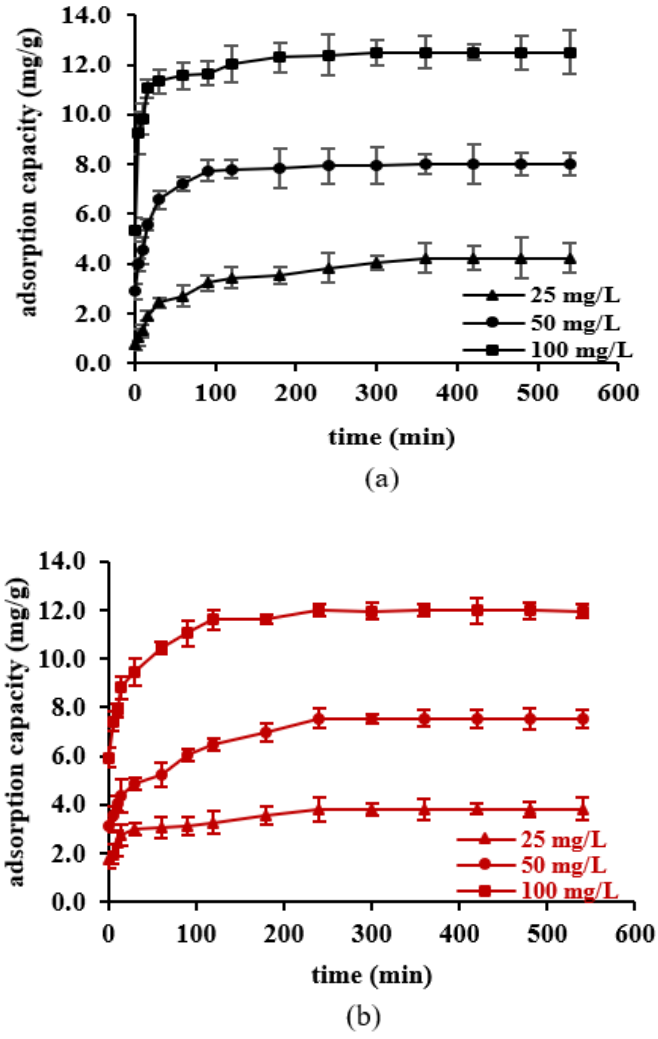

Figure 7 Effect of contact time and initial dye concentration on adsorption of MB (a) and MO (b).

Kinetic studies

To examine the adsorption kinetics, starting dye concentrations of 25, 50 and 100 mg/L were utilized, with contact times ranging from 1 to 540 min. **Figures 8(a) - 8(f)** illustrate the linear graphs for pseudo-first-order kinetics, pseudo-second-order kinetics and intraparticle diffusion kinetics of the adsorption of MB and MO, respectively. **Table 2** displays the computed kinetic parameters.

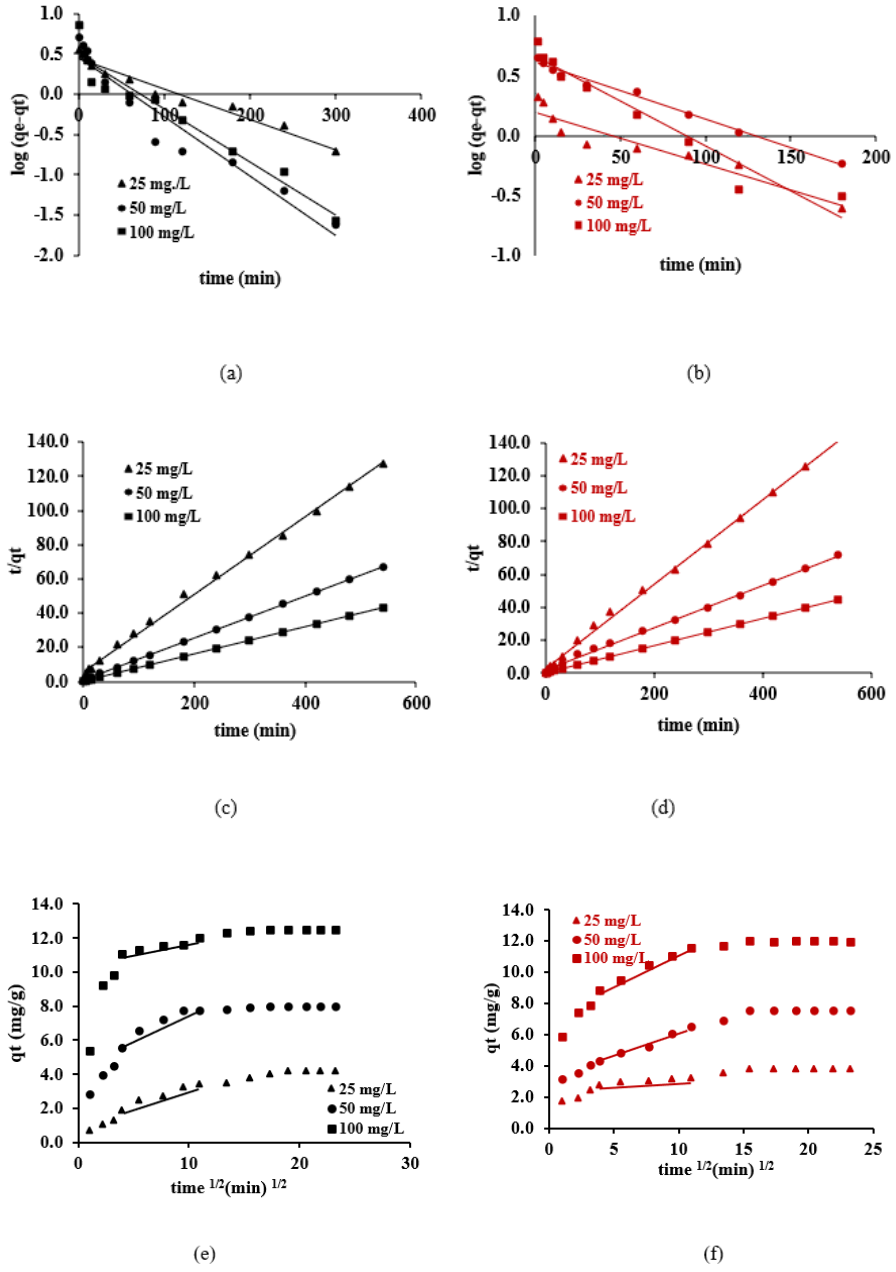

Figure 8 Kinetic models of pseudo-first order (a), (b), pseudo-second order (c), (d), intraparticle diffusion (e), (f) on MB (a), (c), (e) and MO (b), (d), (f) adsorption.

Table 2 Kinetic parameters of MB and MO adsorption onto AC-CR.

Kinetic models	MB dye (mg/L)			MO dye (mg/L)		
	25	**50**	**100**	**25**	**50**	**100**
q_e (exp) (mg/g)	4.231	7.997	12.504	3.384	6.398	11.982
Pseudo-first order						
q_e (mg/g)	2.830	3.049	2.871	1.604	4.045	7.023
k_1 (1/min)	0.009	0.015	0.016	0.010	0.011	0.017
R^2	0.963	0.943	0.925	0.885	0.990	0.954
Δq_e (%)	18.371	25.179	36.130	41.570	29.39	43.80

Kinetic models	MB dye (mg/L)			MO dye (mg/L)		
	25	**50**	**100**	**25**	**50**	**100**
Pseudo-second order						
q_e (mg/g)	4.421	8.097	12.594	3.894	7.770	13.477
k_2 (g/mg·min)	0.009	0.022	0.023	0.025	0.009	0.008
$h = k_2 \cdot q_e^2$ (mg/g·min)	0.176	1.442	3.648	0.379	0.543	1.453
R^2	0.997	0.999	0.999	0.999	0.999	0.999
Δq_e (%)	5.470	2.990	1.560	1.480	2.135	1.060
Intraparticle diffusion						
C (mg/g)	1.155	4.645	10.595	2.692	3.062	4.971
K_{id} (mg/g·min$^{1/2}$)	0.211	0.310	0.124	0.048	0.309	0.711
R^2	0.978	0.933	0.960	0.932	0.961	0.984

Considering the R^2 of the kinetic plots, the R^2 values of the pseudo-second order were nearly close to 1 (> 0.99). Therefore, the kinetic adsorption of MB and MO onto AC-CR was pseudo-second order. Moreover, the calculated q_e values obtained from the pseudo-second order were close to experimental qe values for the adsorption of both dyes. The pseudo-second-order model precisely forecasted the equilibrium adsorption capacities for MB (4.421, 8.097 and 12.594 mg/g) and MO (3.894, 7.770 and 11.960 mg/g) on AC-CR, closely aligning with experimental values (MB: 4.231, 7.997, and 12.504 mg/g; MO: 3.815, 7.542 and 12.121 mg/g). This strong agreement indicated that the adsorption of both dyes followed pseudo-second-order kinetics. Matias *et al*. [41] explained this process as involving liquid membrane expansion, surface adsorption and intraparticle diffusion, often requiring chemical interactions (electron exchange/sharing between dye ions and adsorbent functional groups) for effective adsorption. Similar findings have been observed in the methylene blue and methyl orange dyes on activated carbon prepared from apricot stones and commercial activated carbon [33]. The pseudo-first-order and pseudo-second-order models were quantitatively validated using the normalized standard deviation, Δq_e (%). **Table 2** indicates that the pseudo-second-order model provided a superior fit, as evidenced by lower Δq_e (%) values compared to the pseudo-first-order model across all initial dye concentrations. The findings demonstrate that the pseudo-second-order model provides a more precise representation of the adsorption kinetics of the MB and MO dyes. As the dye concentration grows, the h value, indicating the original rate constant, similarly increases. This implies that the adsorption process of MB and MO on AC-CR involves electrostatic attraction, ion-exchange interactions and π-π bonding [42].

Figures 8(e) - **8(f)** depict the plots of the intraparticle diffusion model for MB and MO adsorption, demonstrating three stages of adsorption: Film diffusion adsorption, intraparticle diffusion adsorption and equilibrium adsorption. The first stage, known as film diffusion, signifies surface adsorption. The second stage, intraparticle diffusion, is the slow step of the diffusion of adsorbates to the inner holes of the adsorbent. The intraparticle diffusion plot's linearity does not pass through the origin, indicating that intraparticle diffusion is not the sole factor influencing adsorption. Other rate-limiting factors beyond intraparticle diffusion are involved in the adsorption process. Consequently, film diffusion also plays a role in regulating the adsorption process [43].

Isotherm of adsorption

The adsorption isotherms for MB and MO dyes on activated carbon at different initial dye concentrations (25 - 200 mg/L) were examined at equilibrium time, with the adsorption data presented in **Figure 9**. **Figure 9** demonstrates the alignment between the nonlinear isotherms of the Langmuir and Freundlich models. The

nonlinear curves were generated utilizing the Solver feature in Excel. **Table 3** presents the linear plot characteristics of the Langmuir and the Freundlich isotherms. The correlation coefficient (R^2) value in **Table 3** demonstrates a strong correlation between the experimental adsorption data and the Langmuir isotherm, indicating that the Langmuir model, with correlation coefficients of 0.968 and 0.986 for MB and MO dyes, respectively, is more accurate than the Freundlich isotherm. Similarly, Rangu *et al.* [29] investigated the adsorption of methylene blue and methyl orange using activated carbon derived from waste tire. Additionally, the adsorption separation factor (R_L) values ranged from 0.085 to 0.513 for MB and from 0.238 to 0.714 for MO, as indicated in **Table 3**. The results demonstrated that the adsorption of MB and MO onto AC-CR was favorable, with R_L values between 0 and 1. The Freundlich isotherm yielded a K_F value of 7.037 and 3.235 and a 1/n value of 0.340 and 0.515 for MB and MO. The 1/n value, ranging from 0 to 1, signified effective adsorption [12].

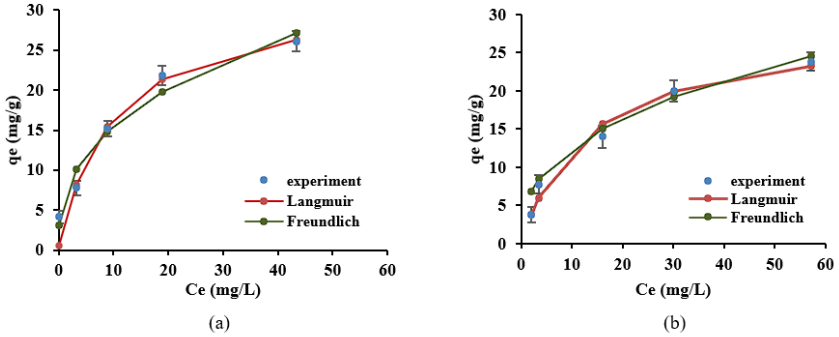

Figure 9 Equilibrium and isotherm of MB (a) and MO (b) dye adsorption onto AC-CR.

Table 3 Isotherm parameters of MB and MO dyes adsorption onto AC-CR.

Isotherm models	values	
	MB dye	**MO dye**
Langmuir isotherm		
q_{max} (mg/g)	29.154	28.736
K_L (L/g)	0.170	0.016
R_L	0.513 - 0.085	0.714 - 0.238
R^2	0.968	0.986
Freundlich isotherm		
K_F (L/mg)	7.034	3.235
1/n	0.340	0.515
R^2	0.947	0.955

Thermodynamic parameters

Thermodynamic investigations of MB and MO adsorption onto AC-CR were performed under equilibrium conditions at constant temperatures of 20, 30 and 40 °C, using an initial dye concentration of 50 mg/L. The equilibrium data were employed to calculate the Gibbs free energy change (ΔG) as described in Eq. (12). The enthalpy (ΔH) and entropy (ΔS) changes were

determined from the slope and intercept of the linear plot of log (q_e/C_e) versus 1/T, as shown in **Figure 11**. The resulting thermodynamic parameters are summarized in **Table 4**.

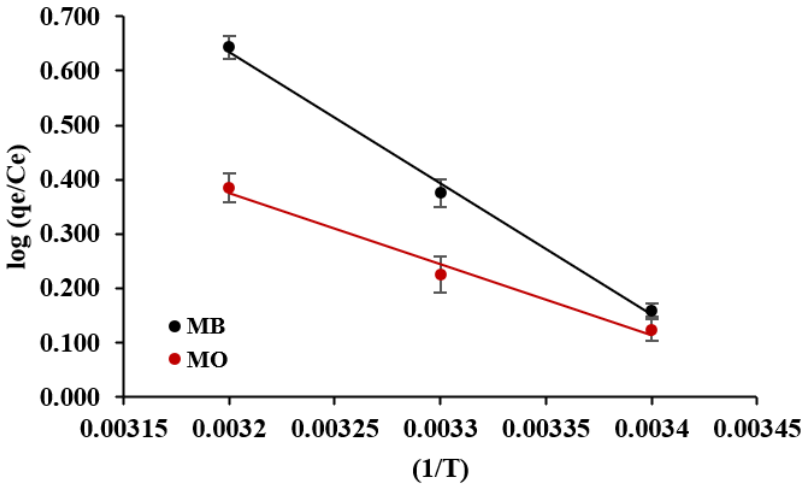

Figure 11 Thermodynamics of MB and MO dyes on AC-CR.

Table 4 Thermodynamic parameters of dyes adsorption onto AC-CR.

Dyes	Temp. (K)	ΔG^0 (kJ/mol)	ΔH^0 (kJ/mol)	ΔS^0 (kJ/mol K)
MB	293	−0.898	40.556	0.141
	303	−2.179		
	313	−3.731		
MO	293	−0.695	25.010	8.702
	303	−1.309		
	313	−2.234		

Table 4 demonstrates that the ΔG values are negative for the initial dye concentration of 50 mg/L at all temperatures. The negative ΔG value indicates that the adsorption process is more favorable and spontaneous. Enhanced adsorption occurs more readily at elevated temperatures, as the adsorbate molecules collide with the active sites of AC-CR more intensely. The Gibbs free energy changes (ΔG) for chemical adsorption typically vary from –80 to –400 kJ/mol, while for physical adsorption, the range is from 0 to –20 kJ/mol [44]. The MB and MO adsorption onto AC-CR can thus be ascribed to physisorption, the primary mechanism in the adsorption process. **Table 4** indicates that the estimated ΔH value is positive, signifying that the adsorption process is endothermic. This suggests that the adsorption is beneficial at higher temperatures. Adsorption is an endothermic process, indicating that dye molecules require increased energy to penetrate the micropores of activated carbon at elevated temperatures [45]. According to Lafi *et al*. [46], the ΔH value is about 40 kJ/mol, and its adsorption mechanism is coordination exchange. Souad and Nadir [47] said that endothermic adsorption was primarily governed by the interaction between the adsorbent and pre-adsorbed water, rather than the interaction between the dye and adsorbent. The positive value of ΔS signifies an increase in entropy. The occurrence is due to the adsorption process increasing the randomness of the solid-solution interface between the adsorbent and the adsorbate solution [1]. Ali *et al*.[10] assert that at the solid-liquid interface, increased adsorption leads to heightened unpredictability and a positive entropy value, attributable to the enhancement of rotational distribution and translational energy.

Adsorbent reusability

To enhance the performance of AC-CR, MB and MO were initially adsorbed, followed by a cleaning process using 0.1 M HCl for MB and 0.1 M NaOH for MO. The regenerated AC-CR was then utilized to adsorb MB and MO individually at a concentration of 50 mg/L, with the adsorption percentage calculated using Eq. (2).

In **Figure 12**, the removal percentages for MB dye during the first through fifth treatments were 90.20%, 82.72%, 69.58%, 63.28% and 55.30%, respectively. Similarly, for MO dye, the removal percentages in the corresponding treatments were 88.82%, 80.22%, 68.23%, 62.28% and 50.46%.

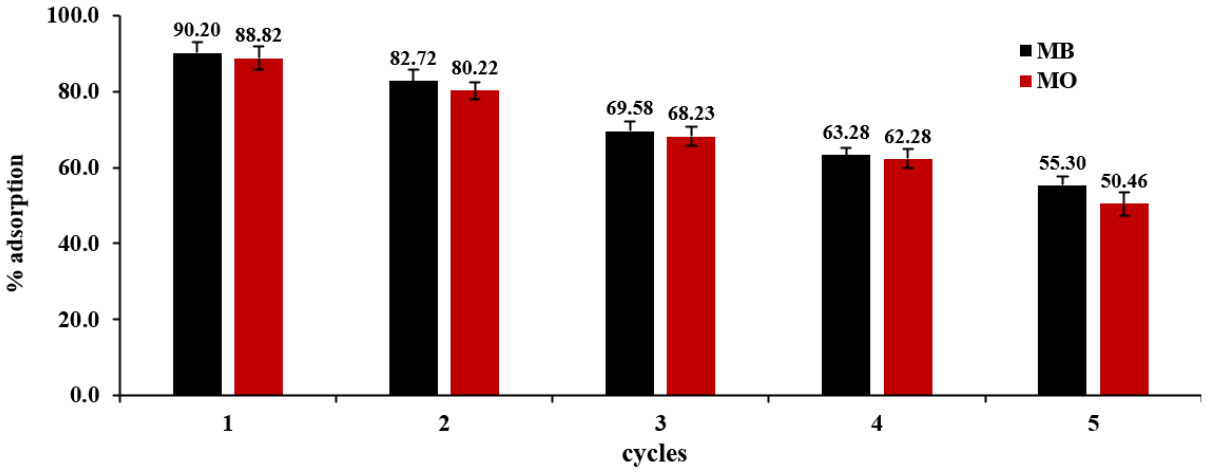

Figure 12 Reusability performance of AC-CR in terms of dye adsorption (%).

Possible adsorption mechanism of MB and MO dye onto AC-CR

Based on the FTIR data and the identified functional groups, including OH, C-O, C=O and COOH, found in the AC-CR. These functional groups possess oxygen atoms with lone pair (n) electrons. The plausible mechanism of MB and MO adsorption on AC-CR is shown in **Figure 13**. Maximum MB adsorption occurs above the pHpzc, increasing negative charge on the adsorbent surface, enhancing the affinity for positively charged molecules (MB^+). The negatively charged areas of the AC-CR surface may demonstrate electrostatic attractions with the cationic dye molecules present in the solution. Maximum MO adsorption happens below the pHpzc, where the positively charged areas of the AC-CR surface may demonstrate electrostatic interactions with the anionic dye molecules (MO^-) present in the solution [15]. Dipole-dipole H-bonding occurs between the hydrogen in the AC-CR surface's –OH group and the dye molecules' nitrogen. As seen from FTIR results (**Figure 5**), the peak of the OH group at 3,746 cm^{-1} shifted to 3,749 cm^{-1} and the intensity of the –OH groups in AC-CR spectra changed slightly after the adsorption of MB and MO. This confirms that hydrogen bonding plays a crucial role in the adsorption mechanism. Furthermore, the Yoshida hydrogen bonding interaction occurs between the hydrogen atoms of the –OH groups on the AC-CR surface and the π-electrons of the aromatic MB and MO rings.

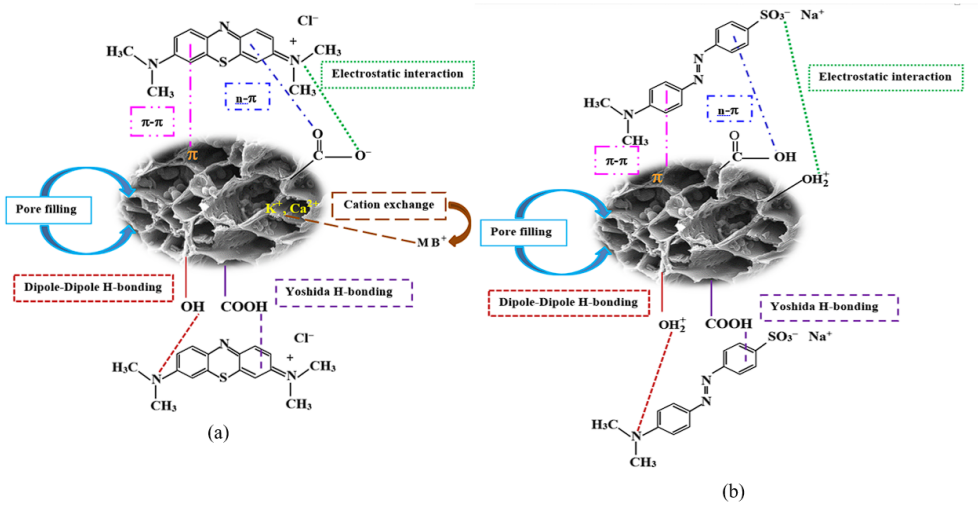

Figure 13 Plausible adsorption mechanism of MB (a) and MO (b) dyes on AC-CR.

The lone pair electron (n) of oxygen on the surface of AC-CR functions serves as a donor in electron donor-acceptor interactions (n–π). In contrast, the π-electron in the aromatic rings of the MB and MO dye molecule serves as an acceptor. The FTIR wavenumber peaks for C=O (1,698 cm^{-1}) and C–O (1,575 cm^{-1}) change to 1,694 and 1,582 cm^{-1} for MB adsorption, while the peaks shift to 1,682 and 1,574 cm^{-1} for MO adsorption, suggesting that n–π interactions may have significantly contributed to the adsorption process [48]. The π-π interactions occur between the π electron system (C=O and C=C) of activated carbon and the π electrons of the MB and MO dye molecules within their aromatic rings. The interactions are shown by the change in the wavelength of the C=C bond peaks, moving from 1,575 to 1,582 cm^{-1} for MB and from 1,575 to 1,574 cm^{-1} for MO dye [42]. Moreover, the absorption band at 757 cm^{-1} of AC-CR shifts to 753 and 746 cm^{-1} upon the adsorption of MB and MO, respectively, confirming the involvement of π-electron interactions within the aromatic rings of the AC-CR surface.

AC-CR is a porous material with pore sizes exceeding 2 µm, as revealed by SEM analysis. The internal pore diameters determined by the BET and BJH methods were 6.282 and 3.696 nm, respectively, indicating that both MB and MO molecules can access the pore structure of AC-CR. The enhanced adsorption capacity is attributed to a concentration gradient effect, which is consistent with the results of intraparticle diffusion studies conducted at various concentrations (**Figure 8**). Consequently, MB and MO are likely adsorbed predominantly via a pore-filling mechanism [16]. Additionally, XRF analysis showed a reduction in Ca and Fe contents after MB adsorption, suggesting that cation exchange occurs between dye molecules and the native cations on the AC-CR surface [49].

In summary, adsorption operates by various mechanisms, including Yoshida hydrogen bonding, dipole-dipole hydrogen bonding, π-π interaction, n-π interaction, electrostatic interaction, pore filling, and ion exchange. These factors may also be significant in the adsorption of MB and MO.

Comparison of cassava residue and other adsorbents for MB and MO adsorption

Table 5 presents the results of a comparative examination of the Langmuir adsorption capacities of MB and MO dyes using different cassava residues and alternative adsorbents. Although previous research has employed waste materials from cassava for dye removal, the application of cassava rhizomes for the removal of MB and MO colors is still restricted. The chemical synthesis of activated carbon from cassava rhizomes is little documented in scholarly literature. This work illustrates that phosphoric acid-activated carbon derived from cassava rhizome is superior in dye removal efficacy compared to alternative adsorbents. As shown in **Table 5**, AC-CR exhibits a comparatively lower maximum adsorption capacity than several other adsorbents. However, its capacity for MB adsorption surpasses that of commercial activated carbon [52], teak sawdust-derived activated carbon [54] and cassava peel

biochar [53]. In the case of MO, its maximum adsorption capacity is lower than that of commercial activated carbon [56], but still exceeds that of *Prosopis juliflora* waste biochar [59].

Table 5 Comparison of the maximum adsorption of MB and MO dyes on various adsorbents.

Adsorbents	Dyes	q_{max} (mg/g)	References
Cassava rhizome-activated carbon ($ZnCl_2$)	MB	274	[50]
Calicotome villosa activated carbon	MB	169.78	[51]
Commercial activated carbon	MB	15.24	[52]
Cassava peel biochar	MB	4.75	[53]
Teak Sawdust-Derived Activated Carbon	MB	13.48	[54]
Cassava Rhizome-activated carbon (H_3PO_4)	MB	29.15	This work
Carbon material	MO	285.71	[55]
Commercial activated carbon	MO	113	[56]
P(VDF-TrFE)/MWCNTs/K) nanocomposite	MO	62.89	[57]
Anchote peel-based agricultural waste	MO	103.03	[58]
Prosopis juliflora waste biochar	MO	8.08	[59]
Cassava Rhizome-activated carbon (H_3PO_4)	MO	28.74	This work

Binary adsorption test

The residual concentrations of MB and MO in the binary system were quantified using Eqs. (14) - (15). These values were subsequently analyzed using the Ideal Adsorbed Solution Theory (IAST), which assumes that all mixture components behave as ideal adsorbed solutes, implying no interactions between the adsorbates and the adsorbent [60]. Binary adsorption tests were conducted using three sets of MB and MO solution mixtures at concentration ratios of 1:1, 1.5:1 and 1:1.5. The combined equilibrium concentrations from each set were applied in the IAST model. **Figure 14** presents the adsorption concentrations (mol/L) of each component (MB and MO) in the respective experiments (Exp1, Exp2 and Exp3), alongside the corresponding IAST predictions (IAST1, IAST2 and IAST3). The IAST calculations were carried out using Excel Solver.

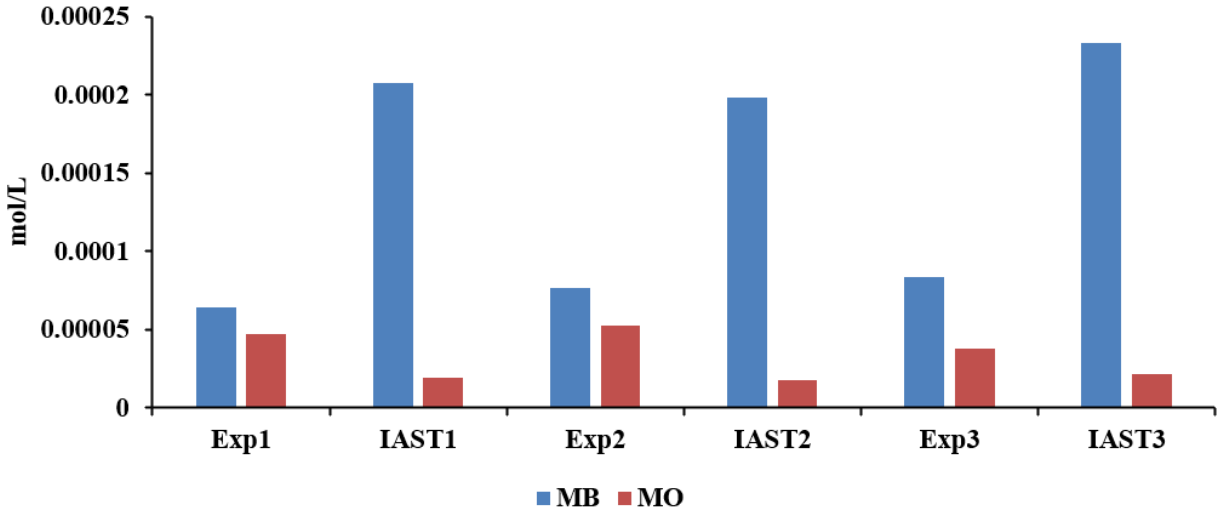

Figure 14 Binary dye adsorption performance of AC-CR (MB and MO).

Figure 14 illustrates that methylene blue (MB) exhibited higher adsorption capacity than methyl orange (MO) in all binary adsorption experiments (Exp1, Exp2 and Exp3). The IAST model analysis revealed a trend consistent with the experimental results, indicating that MB exhibits higher adsorption than MO; however, the predicted values deviated from the experimental data. The IAST simulations indicated an overestimation of MB adsorption and an underestimation of MO, reflecting a disparity between predicted and observed values. This discrepancy suggests that the IAST model was unable to provide an accurate prediction of the binary adsorption behavior in this system.

Cost analysis

The utilization of agricultural waste, such as cassava rhizome, for activated carbon production enhances waste valorization, mitigates environmental impact and supports circular economy principles. This study transforms a low-cost precursor into high-value activated carbon for the effective removal of pollutants, specifically methylene blue (MB) and methyl orange (MO). The resulting AC-CR demonstrates significant economic and environmental advantages due to its straightforward preparation process. Beyond MB and MO removal, the prepared AC-CR exhibits potential for broader environmental remediation applications. Additionally, its durability, reusability and reduced environmental footprint contribute to its long-term cost-effectiveness.

Conclusions

This study demonstrated the effective utilization of cassava rhizome-derived activated carbon (AC-CR), synthesized through H_3PO_4 activation at 500 °C, as a low-cost mesoporous adsorbent for the removal of methylene blue (MB) and methyl orange (MO) from aqueous solutions. AC-CR exhibited a BET surface area of 19.738 m^2/g with a predominant pore size distribution within the mesoporous range, confirming its suitability for dye adsorption. Optimal removal efficiencies were achieved at pH 9 for MB and pH 2 for MO. The adsorption equilibrium data conformed well to the Langmuir isotherm model, indicating monolayer adsorption, while the kinetic behavior followed a pseudo-second-order model, suggesting chemisorption as the rate-limiting step. Temperature dependence further revealed an endothermic and spontaneous adsorption process. FTIR characterization and Boehm titration indicated the presence of hydroxyl, carbonyl, and carboxylic groups, supporting the involvement of multiple adsorption mechanisms. Furthermore, AC-CR demonstrated high regeneration efficiency over five cycles using HCl (for MB) and NaOH (for MO), maintaining substantial adsorption capacity. Its successful application in binary dye adsorption further underscores its potential as a sustainable and economical solution for dye-laden wastewater treatment.

Acknowledgements

Thepsatri Rajabhat University, Thailand provided support for this study, for which the authors are grateful.

Declaration of Generative AI in Scientific Writing

We have used QuillBot and Grammarly for checking the grammar and paraphrasing the written sentences.

CRediT Author Statement

Sawasdee, S.: Conceptualization, Methodology, Formal analysis, Data Curation, Writing - Original Draft, Project Administration. **Watcharabundit, P.**: Writing - Review & Editing, Visualization.

References

[1] NUM Nizam, MM Hanafiah, E Mahmoudi, AA Halim and AW Mohammad. The removal of anionic and cationic dyes from an aqueous solution using biomass-based activated carbon. *Scientific Reports* 2021; **11**, 8623.

[2] S Moosavi, CW Lai, S Gan, G Zamiri, OA Pivehzhani and MR Johan. Application of efficient magnetic particles and activated carbon for dye removal from wastewater. *ACS Omega* 2020; **5(33)**, 20684-20697.

[3] K Kouhi, A Amouei, H Asgharnia, M Vosoughi, SH Fallah and M Shirmardi. Application of oak charcoal-based activated carbon for the removal of methylene blue dye from aqueous solutions: Kinetics, equilibrium and reusability studies. *Water Practice & Technology* 2023; **18(12)**, 3255-3270.

[4] SP Mishra, AR Patra and S Das. Methylene blue and malachite green removal from aqueous solution using waste activated carbon. *Biointerface Research in Applied Chemistry* 2021; **11(1)**, 7410-7421.

[5] D Dimbo, M Abewaa, E Adino, A Mengistu, T Takele, A Oro and M Rangaraju. Methylene blue adsorption from aqueous solution using activated carbon of *spathodea campanulata*. *Results in Engineering* 2024; **21**, 101910.

[6] GV Serban, VI Iancu, C Dinu, A Tenea, N Vasilache, I Cristea, M Niculescu, I Ionescu and FL Chiriac. Removal efficiency and adsorption kinetics of methyl orange from wastewater by commercial activated carbon. *Sustainability* 2023; **15(17)**, 12939.

[7] J Fito, M Abewaa, A Mengistu, K Angassa, AD Ambaye, W Moyo and T Nkambule. Adsorption of methylene blue from textile industrial wastewater using activated carbon developed from rumex abyssinicus plant. *Scientific Reports* 2023; **13(1)**, 5427.

[8] MC Silva, L Spessato, TL Silva, GK Lopes, HG Zanella, JT Yokoyama, AL Cazetta and VC Almeida. H_3PO_4–activated carbon fibers of high surface area from banana tree pseudo-stem fibers: Adsorption studies of methylene blue dye in batch and fixed bed systems. *Journal of Molecular Liquids* 2021; **324**, 114771.

[9] Z Heidarinejad, MH Dehghani, M Heidari, G Javedan, I Ali, and M Sillapaa. Methods for preparation and activation of activated carbon: A review. *Environmental Chemistry Letters* 2020; **18**, 393-415.

[10] NS Ali, NM Jabbar, SM Alardhi, HS Majdi and TM Albayati. Adsorption of methyl violet dye onto a prepared bio-adsorbent from date seeds: Isotherm, kinetics and thermodynamic studies. *Heliyon* 2022; **8(8)**, e10276.

[11] IH Dakhil and AH Ali. Adsorption of methylene blue dye from industrial wastewater using activated carbon prepared from agriculture wastes. *Desalination and Water Treatment* 2021; **216**, 372-378.

[12] SA Mousavi, D Shahbazi, A Mahmoudi and P Darvishi. Methylene blue removal using prepared activated carbon from grape wood waste: Adsorption process analysis and modeling. *Water Quality Research Journal* 2022; **57(1)**, 1-19.

[13] S Kanyakam, W Pimpa and P Tansupo. Effects of carbonization temperature on properties of activated carbon prepared from cassava rhizome waste disposal from starch industry. *International Journal of Management and Applied Science* 2017; **3(12)**, 1-3.

[14] J Phuriragpitikhon, K Pluamjai, W Fuangchoonuch and L Chuenchom. Conversion of cassava rhizome into efficient carbonaceous adsorbents for removal of dye in water. Earth and environmental science. *In*: Proceedings of the 13th IMT-GT UNINET BIOSCIENCE International Conference, Songkhla, Thailand. 2022.

[15] YY Tan, AAA Raman, MIIZ Abidin and A Buthiyappan. Sustainable dye adsorption using novel activated carbon prepared from passion fruit (*Passiflora edulis*) leaf: Mechanism and cost analysis. *Industrial & Engineering Chemistry Research* 2023; **62(36)**, 14507-14521.

[16] HN Tran, W Ya-Fen, Y Sheng-Jie and C Huan-Ping. Insights into the mechanism of cationic dye adsorption on activated charcoal: The importance of π–π interactions. *Process Safety and Environmental Protection* 2017; **107**, 168-180.

[17] P Chukaew, K Nakason, S Kuboon, W Kraithong, B Panyapinyopol and V Kanokkantapong. Conversion of cassava rhizome to biocrude oil via hydrothermal liquefaction. *International Energy Journal* 2021; **21(3)**, 269-280.

[18] K Nakason, P Khemthong, W Kraithong, P Chukaew, B Panyapinyopol, D Kitkaew and P Pavasant. Upgrading properties of biochar fuel derived from cassava rhizome via torrefaction: Effect of sweeping gas atmospheres and its economic feasibility. *Case Studies in Thermal Engineering* 2021; **23**, 100823.

[19] V Gajendiran, P Deivasigamani, S Sivamani and PM Sivakumar. A review on cassava residues as adsorbents for removal of organic and inorganic contaminants in water and wastewater. *Journal of Chemistry* 2023; **2023**, 7891518.

[20] A Kurniawan, AN Kosasih, J Febrianto, YH Ju, J Sunarso, N Indraswati and S Ismadji. Evaluation of cassava peel waste as lowcost biosorbent for Ni-sorption: Equilibrium, kinetics, thermodynamics

and mechanism. *Chemical Engineering Journal* 2011; **172(1)**, 158-166.

[21] NF Al-Harby, EF Albahly and NA Mohame. Kinetics, isotherm and thermodynamic studies for efficient adsorption of congo red dye from aqueous solution onto novel cyanoguanidine-modified chitosan adsorbent. *Polymers* 2021; **13(24)**, 4446.

[22] N Atar, A Olgun, S Wang and S Liu. Adsorption of anionic dyes on boron industry waste in single and binary solutions using batch and fixed-bed systems. *Journal of Chemical & Engineering Data* 2011; **56(3)**, 508-516.

[23] QT Tran, TH Do, XL Ha, TTA Duang, Mn Chu, VN Vu, HD Chau, TKN Tran and P Song. Experimental design, equilibrium modeling and kinetic studies on the adsorption of methylene blue by adsorbent: Activated carbon from durian shell waste. *Materials Research* 2022; **15**, 8566.

[24] A Kumar, S Prasad, PN Saxena, NG Ansari and DK Patel. Synthesis of alginate-based Fe_3O_4-MnO_2 xerogel and its application for the concurrent elimination of Cr(VI) and Cd(II) from aqueous solution. *ACS Omega* 2021; **6**, 3931-3945.

[25] H Li, L Liu, J Cui, F Wang and F Zhang. High-efficiency adsorption and regeneration of methylene blue and aniline onto activated carbon from waste edible fungus residue and its possible mechanism. *RSC Advances* 2020; **10(24)**, 14262-14273.

[26] S Fu, Q Fang, A Li, Z Li, J Han, X Dang and W Han. Accurate characterization of full pore size distribution of tight sandstones by low-temperature nitrogen gas adsorption and high-pressure mercury intrusion combination method. *Energy Science & Engineering* 2021; **9(1)**, 80-100.

[27] R Mansour, MG Simeda and A Zaatout. Adsorption studies on brilliant green dye in aqueous solutions using activated carbon derived from guava seeds by chemical activation with phosphoric acid. *Desalination and Water Treatment* 2020; **202**, 396-409.

[28] C Wen, T Liu, D Wang, Y Wang, H Chen, G Luo, Z Zhou, C Li and M Xu. Biochar as the effective adsorbent to combustion gaseous pollutants: Preparation, activation, functionalization and the adsorption mechanisms. *Progress in Energy and Combustion Science* 2023; **99**, 101098.

[29] SD Rangu, PP Mon, PP Cho, UR Mudadla, HS Rangappa, S Duvvuri and S Challapalli. Simultaneous and efficient adsorption of methylene blue and methyl orange by low-cost adsorbent derived from waste tire. *Environmental Science and Pollution Research International* 2025. https://doi.org/10.1007/s11356-025-36122-y

[30] S Biswas and U Mishra. Effective remediation of lead ions from aqueous solution by chemically carbonized rubber wood sawdust: Equilibrium, kinetics and thermodynamic study. *Journal of Chemistry* 2015; **2015(3)**, 1-8.

[31] M Zięzio, B Charmas, K Jedynak, M Hawryluk and K Kucio. Preparation and characterization of activated carbons obtained from the waste materials impregnated with phosphoric acid (V). *Applied Nanoscience* 2020; **10**, 4703-4716.

[32] J Wang, R Wang, J Ma and Y Sun. Study on the application of shell-activated carbon for the adsorption of dyes and antibiotics. *Water* 2022; **14(22)**, 3752.

[33] AS Elkholy, MS Yahia, MA Elnwawy, HA Gomaa and AS Elzaref. Synthesis of activated carbon composited with Egyptian black sand for enhanced adsorption performance toward methylene blue dye. *Scientific Reports* 2023; **13(1)**, 4209.

[34] A Boukir, S Fellak and P Doumenq. Structural characterization of argania spinosa Moroccan wooden artifacts during natural degradation progress using infrared spectroscopy (ATR-FTIR) and x-ray diffraction (XRD). *Heliyon.* 2019; **9(5)**, e02477.

[35] S Hmamouchi, Y Abbad, AE Yacoubi, A Boulouiz, B Sallek and BC El Idrissi. Optimization study of methylene blue dye adsorption on Chamaerops humilis fibers biosorption using a central composite design. *Desalination and Water Treatment* 2024; **320**, 100824.

[36] NV Hung, BTM Nguyet, NH Nghi, NM Thanh, NDV Quyen, VT Nguyen, DN Nhiem and DQ Khieu. Highly effective adsorption of organic dyes

from aqueous solutions on longan seed-derived activated carbon. *Environmental Engineering Research* 2022; **28(3)**, 220116.

[37] DH Nguyen, HN Tran, HP Chao and CC Lin. Effect of nitric acid oxidation on the surface of hydrochars to sorb methylene blue: An adsorption mechanism comparison. *Adsorption Science & Technology* 2019; **37(7-8)**, 607-622.

[38] AA Fakunmoju, F Azaman, A Ai and S Hamzah. Methylene blue adsorption by chemical-activated Trichanthera gigantea leaf. *Water Practice & Technology* 2024; **19(11)**, 4522-4537.

[39] J Zhou, M Li, Y Tao and L Zha. Study on the adsorption characteristics of methylene blue by magnesium-modified fly Ash. *Molecules* 2025; **30(5)**, 992.

[40] A Keereerak and W Chinpa. A potential biosorbent from Moringa oleifera pod husk for crystal violet adsorption Kinetics, isotherms, thermodynamic and desorption studies. *Journal of the Science Society of Thailand* 2020; **46**, 186-194.

[41] CA Matias, LJGGD Oliveira, R Geremias and J Stolberg.Biosorption of rhodamine B from aqueous solution using Araucaria angustifolia sterile bracts. *Revista Internacional de Contaminación Ambiental* 2020; **36(1)**, 97-104.

[42] Q Yao, Y Peng, M Chen, Y wang, J Ding, B Ma, Q Wang, S Lu and S Lu. One-step high efficiency synthesis of zeolite from fly ash by mechanochemical method as a low-cost adsorbent for cadmium removal. *Journal of Environmental Chemical Engineering* 2024; **12(1)**, 111877.

[43] PS Kumar. Adsorption of Zn (II) ions from aqueous environment by surface modified strychnos potatorum seeds, a low-cost adsorbent. *Polish Journal of Chemical Technology* 2013; **15(3)**, 35-41.

[44] A Bazan-Wozniak, J Cielecka-Piontek, A Nosal-Wiercińska and R Pietrzak. Adsorption of organic compounds on adsorbents obtained with the use of microwave heating. *Materials* 2022; **15(16)**, 5664.

[45] MA Al-Ghouti and RS Al-Absi. Mechanistic understanding of the adsorption and thermodynamic aspects of cationic methylene blue dye onto cellulosic olive stones biomass from wastewater. *Scientific Reports* 2020; **10(1)**, 15928.

[46] R Lafi, I Montasser and A Hafiane. Adsorption of congo red dye from aqueous solutions by prepared activated carbon with oxygen-containing functional groups and its regeneration. *Adsorption Science & Technology* 2019; **37(1-2)**, 160-181.

[47] B Souad and M Nadir. Kinetic and thermodynamic study of methyl orange dye adsorption on zinc carbonyldiphthalate, an organometallic-based material prepared with a montmorillonite clay. *Iranian Journal of Chemistry and Chemical Engineering* 2023; **42(1)**, 123-138.

[48] C Poornachandhra, RM Jayabalakrishnan, M Prasanthrajan, G Balasubramanian, A Lakshmanan, S Selvakumar and JE John. Cellulose-based hydrogel for adsorptive removal of cationic dyes from aqueous solution: Isotherms and kinetics. *RSC Advances* 2023; **13(7)**, 4757-4774.

[49] M Turabık and B Gozmen. Removal of basic textile dyes in single and multi-dye solutions by adsorption: Statistical optimization and equilibrium isotherm studies. *CLEAN–Soil, Air, Water* 2013; **41(11)**, 1080-1092.

[50] J Phuriragpitikhon, K Pluamjai, W Fuangchoonuch and L Chuenchom. Conversion of cassava rhizome into efficient carbonaceous adsorbents for removal of dye in water. Earth and Environmental Science. *In*: Proceedings of the 13th IMT-GT UNINET BIOSCIENCE International Conference, Songkhla, Thailand. 2022.

[51] M Ibrahim, M Souleiman and A Salloum. Methylene blue dye adsorption onto activated carbon developed from *Calicotome villosa* via H_3PO_4 activation. *Biomass Conversion and Biorefinery* 2023; **13**, 12763-12776.

[52] RH Khuluk, A Rahmat, Buhani and Suharso. Removal of methylene blue by adsorption onto activated carbon from coconut shell (*Cocos nucifera L.*). *Indonesian Journal of Science and Technology* 2019; **4(2)**, 229-240.

[53] AK Anas, A Izzah, SY Pratama and FI Fajarwati. Removal of methylene blue using biochar from cassava peel (Manihot utilissima) modified by sodium dodecyl sulphate (SDS) surfactant. *AIP Conference Proceedings* 2020; **2229(1)**, 030024.

[54] IGAK Suriadi, DNKP Negara, TGT Nindhia, IKA Atmika, IMDB Penindra and IMG Karohika. The

Impact of activation heating rate on pore structure in Teak Sawdust-Derived activated carbon and its application in methylene blue adsorption. *Trends in Sciences* 2024; **21(9)**, 8110.

[55] Y Dai and J Li. Adsorption behavior of methyl orange and methylene blue onto carbon material in aqueous solution. *Desalination and Water Treatment* 2020; **180**, 387-397.

[56] EHEL Khattabi, Y Rachdi, R Bussam, EH Mourid, Y Naimi, MEL Alouani and S Belaaouada. Enhanced elimination of methyl orange and recycling of an eco-friendly adsorbent activated carbon from aqueous solution. *Russian Journal of Physical Chemistry B* 2021; **15**, S149-S159.

[57] M El-Gamal, FM Mohamed, MA Mekewi, FS Hashem, MR El-Aassar and RE Khalifa. Adsorptive removal of Methyl orange from aqueous solutions by polyvinylidene fluoride tri-fluoro ethylene/carbon nanotube/kaolin nanocomposite: Kinetics, isotherm and thermodynamics. *Desalination and Water Treatment* 2020; **193**, 142-151.

[58] AA Hambisa, MB Regasa, HG Ejigu and CB Senbeto. Adsorption studies of methyl orange dye removal from aqueous solution using Anchote peel-based agricultural waste adsorbent. *Applied Water Science* 2023; **13**, 24.

[59] C Diaz-Uribe, J Ortiz, F Duran, W Vallejo and J Fals. Methyl orange adsorption on biochar obtained from *Prosopis juliflora* waste: Thermodynamic and kinetic study. *ChemEngineering* 2023; **7**, 114.

[60] AJ Jadhav and C Srivastava. Adsorbed solution theory based modeling of binary adsorption of nitrobenzene, aniline and phenol onto granulated activated carbon. *Chemical Engineering Journal* 2013; **229**, 450-459.